MICROSTRUCTURE AND PROPERTIES

This chapter describes the results on microstructure and properties of Cu-4 wt.% Ni –TiC composites produced by high energy ball milling, followed by compaction and sintering. The results have been discussed comprehensively on the basis of observed microstructure, the amount of TiC and the processing parameters.

4.1 RESULTS

4.1.1 Microstructure of mechanically alloyed (MA) powder

The various powders such as Cu, Ni and TiC used for synthesizing the composites have been characterized by using SEM and X-ray diffraction in regard to their shape and size. Figures 4.1(a) and (b) show the SEM micrograph and X-ray diffraction (XRD) pattern of the as-received copper powder, respectively. The copper powder (Cu) has a dendritic structure as evident from Fig. 4.1 (a). Three major peaks of Cu (111), (200), and (220) having a cubic crystal structure and lattice parameter a = 3.615 Å could be indexed by matching with the JCPDS # 85-1326 as shown in Fig. 4.1 (b). Figure 4.2 (a) presents the morphology and Fig. 4.2 (b) depicts X-ray diffraction pattern of nickel (Ni) powder.

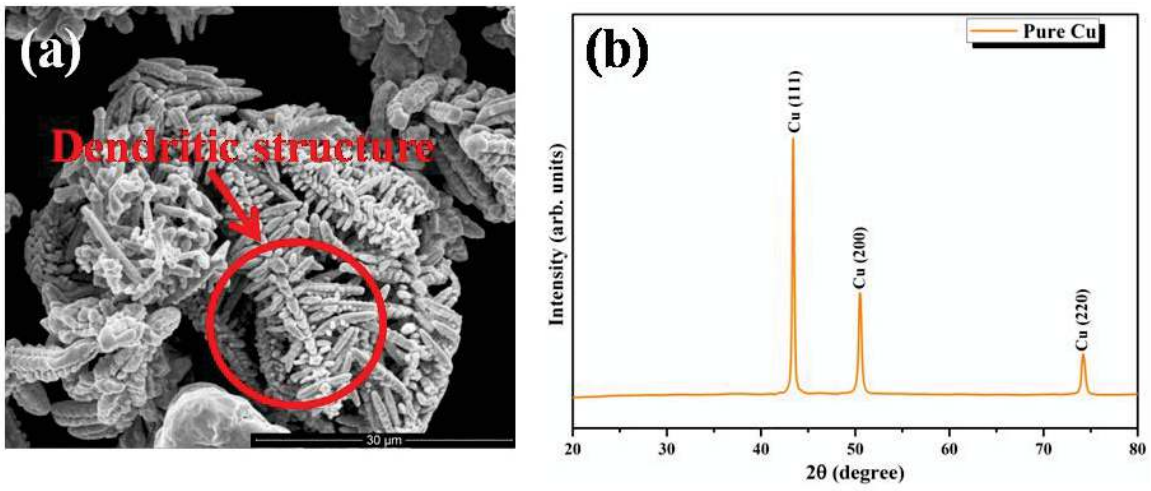

Fig.4.1: (a) The morphology and (b) X-ray diffraction pattern of as-received Cu powder.

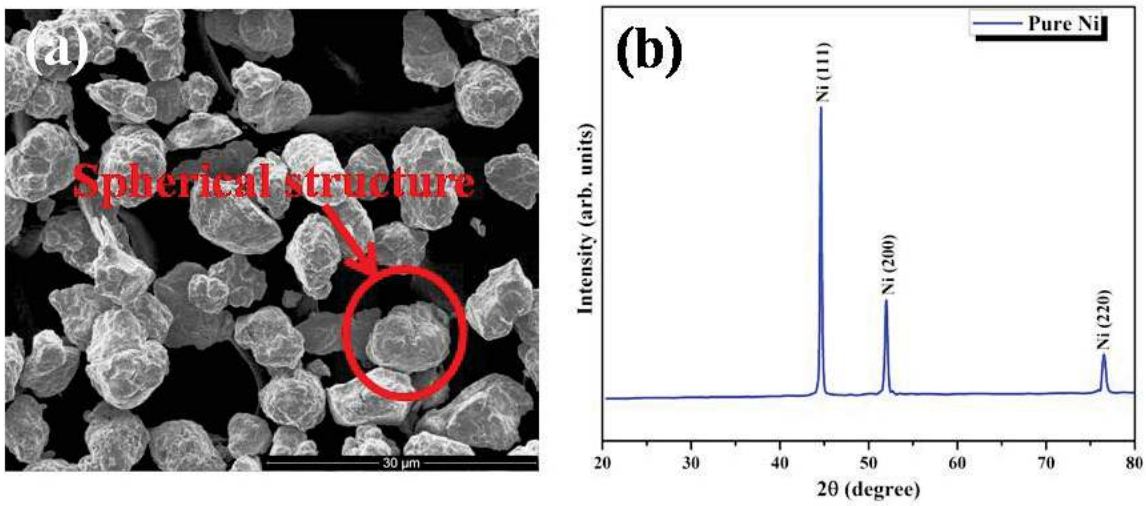

Fig.4.2: (a) The morphology and (b) X-ray diffraction pattern of Ni powder.

It is clear from the micrograph that the nickel powder has nearly spherical shaped structure. The X-ray diffraction (XRD) pattern of Ni powder is presented in Fig.4.2 (b). Peaks of nickel in the XRD were matched with JCPDS # 04-0850. Titanium carbide powder (TiC) presents a sharp-edged type structure as shown in Fig 4.3 (a). All the five peaks as shown in Fig.4.3 (b), were identified as reflections from the (111), (200), (220), (311) and (221)) planes of TiC having a lattice parameter, a = 4.317 Å. The peaks of TiC in the XRD were matched with JCPDS # 89-3828.

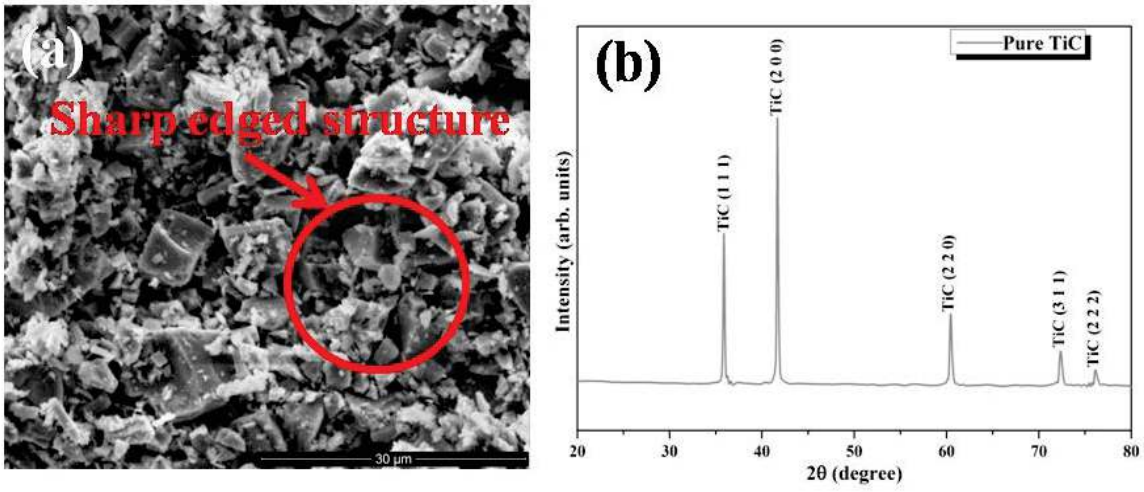

Fig.4.3: (a) The morphology and (b) X-ray diffraction pattern of TiC powder.

Figures 4.4 (a) to (e) show the SEM morphology of (a) Cu4Ni, (b) Cu4Ni-2TiC, (c) Cu4Ni-4TiC, (d) Cu4Ni-6TiC and (e) Cu4Ni-8TiC composite powders milled for 6 h. It is observed that particle size is bigger in Fig. 4.4 (a) as compared to the other composite powders as shown in Figs. 4.4 (b) to (e). As the weight percentage of TiC increases in the matrix alloy, its powder particle size decreases up to 4 wt.% TiC content and there after the particle size increases as the TiC content is increased to 6 and 8 wt.%.

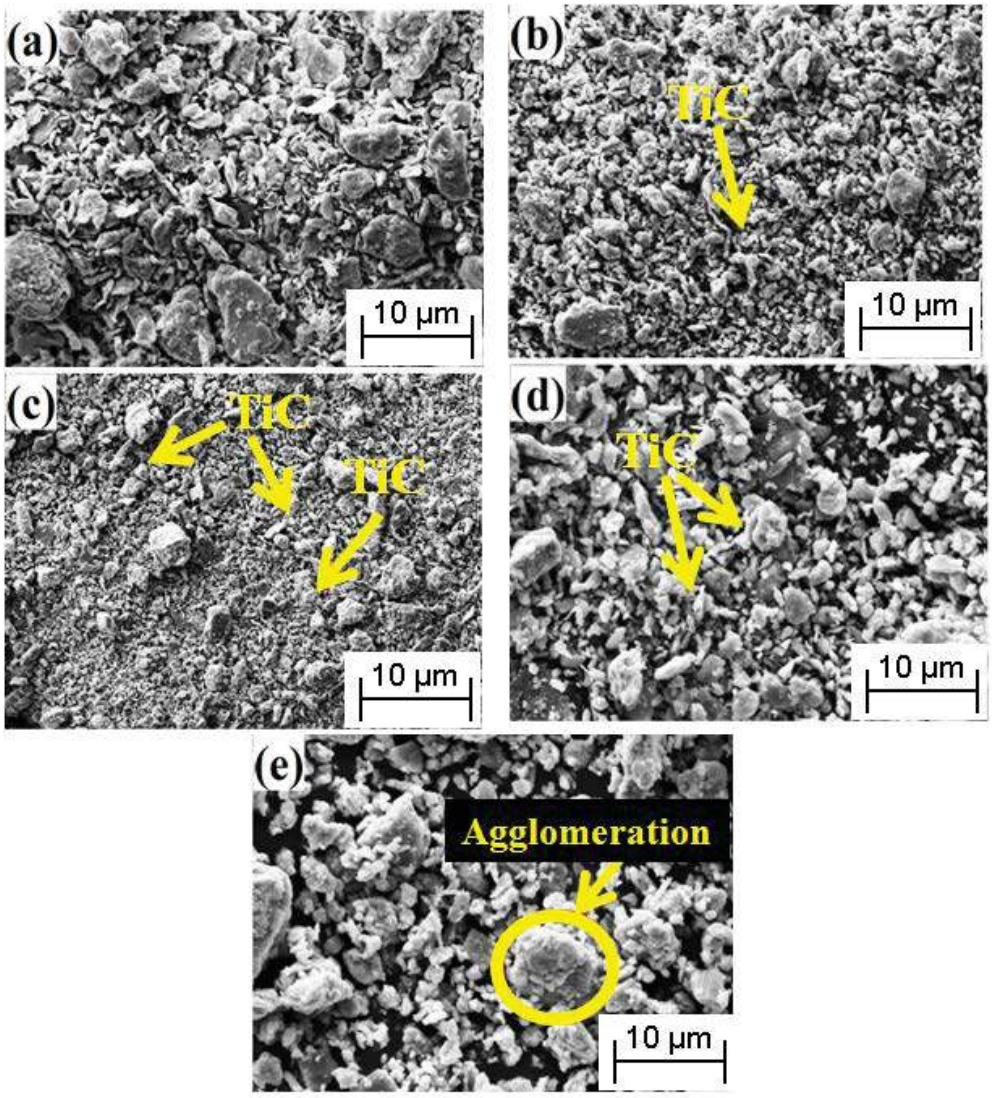

Fig.4.4: The SEM morphology of (a) Cu4Ni, (b) Cu4Ni-2TiC, (c) Cu4Ni-4TiC, (d) Cu4Ni- 6TiC and (e) Cu4Ni-8TiC composite powders milled for 6 h.

Figures 4.4 (b) to (e) show that titanium carbide particles are distributed uniformly in the matrix as marked by arrows in respective micrographs. The particle size distribution of composite powders as a function of reinforcement is illustrated in the histograms given in Figures 4.5 (a) to (e) which also confirms the reduction in the particle size with increasing TiC content.

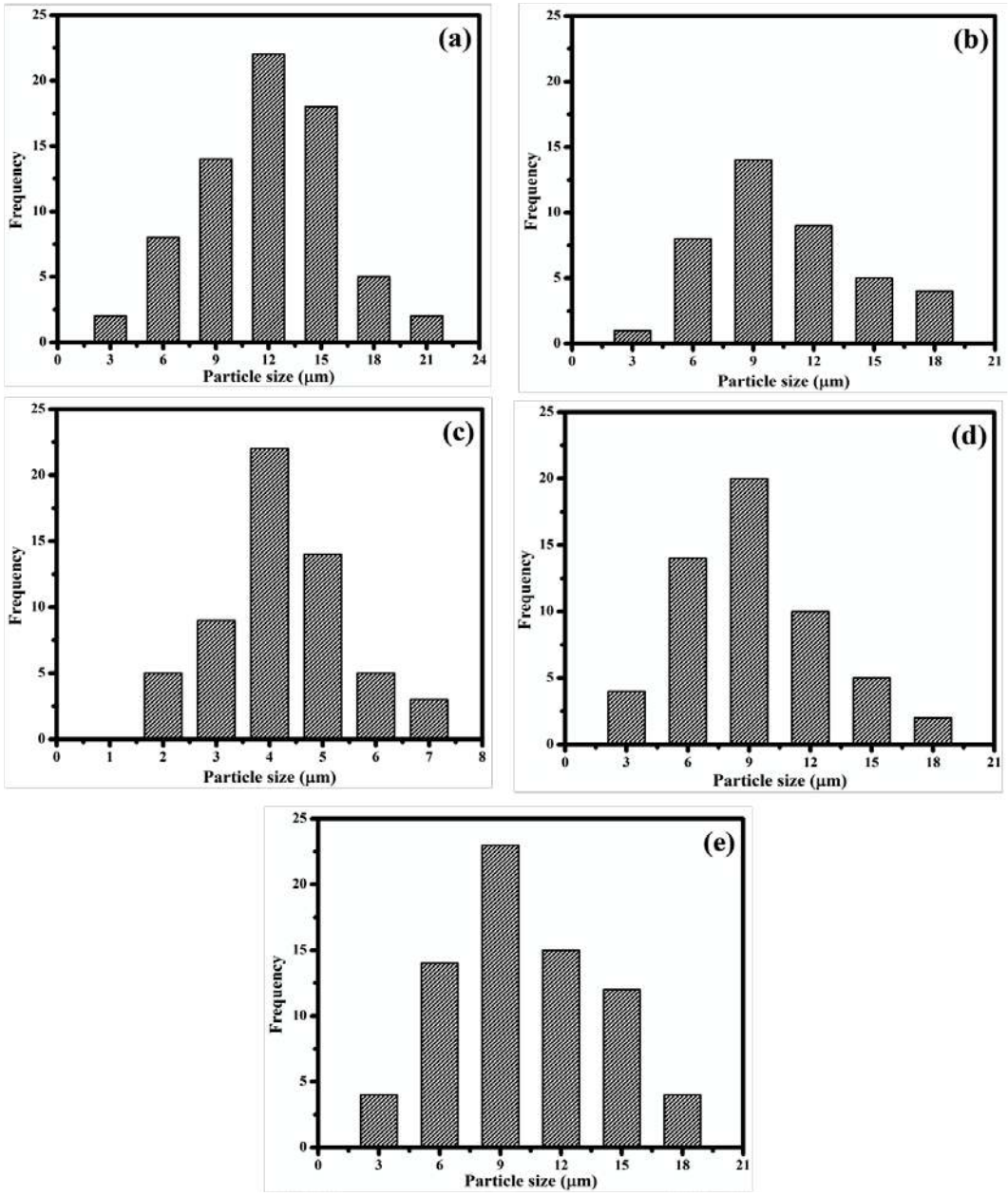

Fig 4.5: Particle size distribution for (a) Cu4Ni, (b) Cu4Ni-2TiC, (c) Cu4Ni-4TiC, (d) Cu4Ni-6TiC and (e) Cu4Ni-8TiC powder after 6 h of milling.

Figures 4.6 (a) to (d) show the change in powder morphology typically for Cu4Ni-4TiC composite powder with different milling durations i.e., 0, 2, 4 and 6 h. The shape of the particles has been observed to change from flaky to equiaxed as marked on the micrographs. Similar, features have been observed for other composite powders, hence, those have not been included here. Figures 4.7 (a) through (d) depict the particle size distribution as a function of milling time for Cu4Ni-4TiC composite powder for 0, 2, 4 and 6 h of milling. The size of the particles is found to reduce with increasing time of milling duration as evident from histograms shown in Fig. 4.7 (a) through (d).

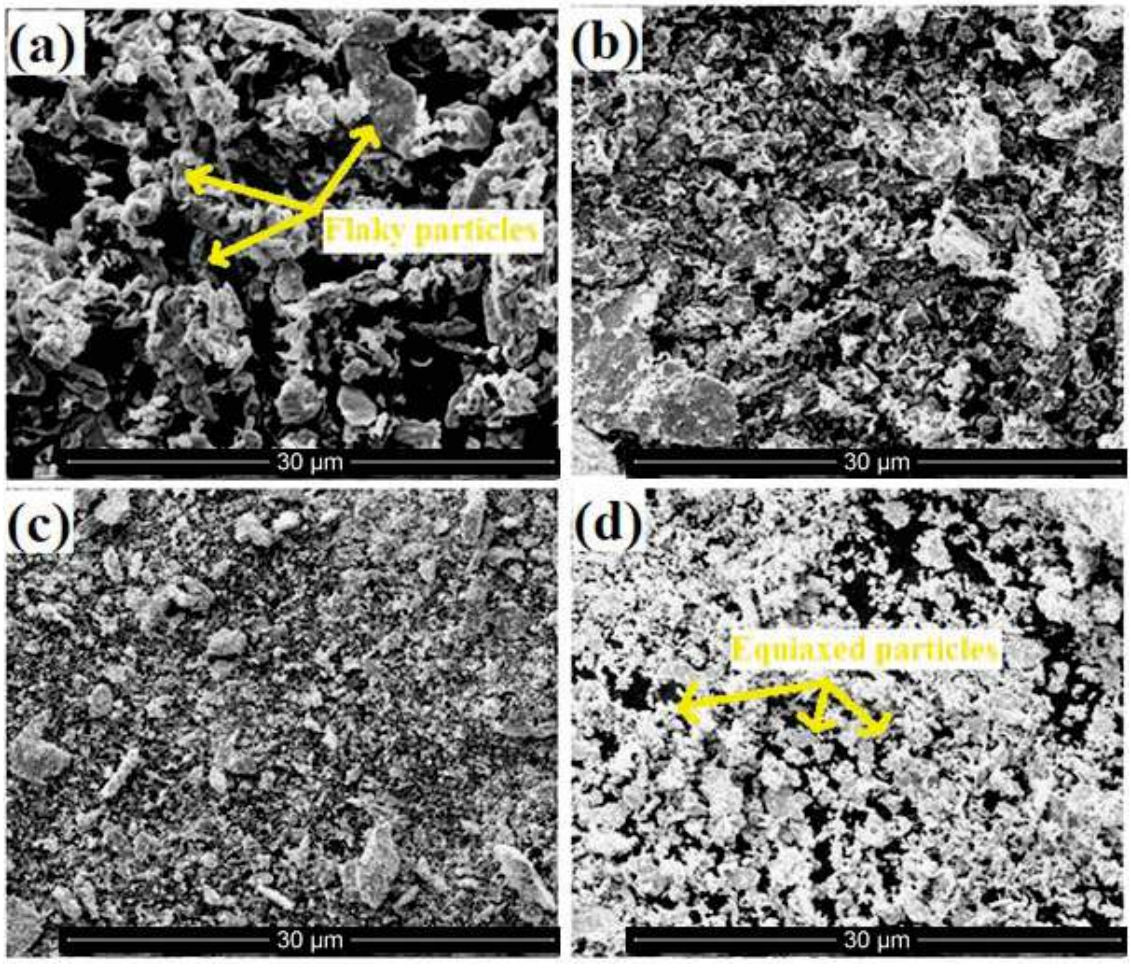

Fig 4.6: The morphology of Cu4Ni-4TiC composite powder after (a) 0 h, (b) 2 h, (c) 4 h and (d) 6 h of milling.

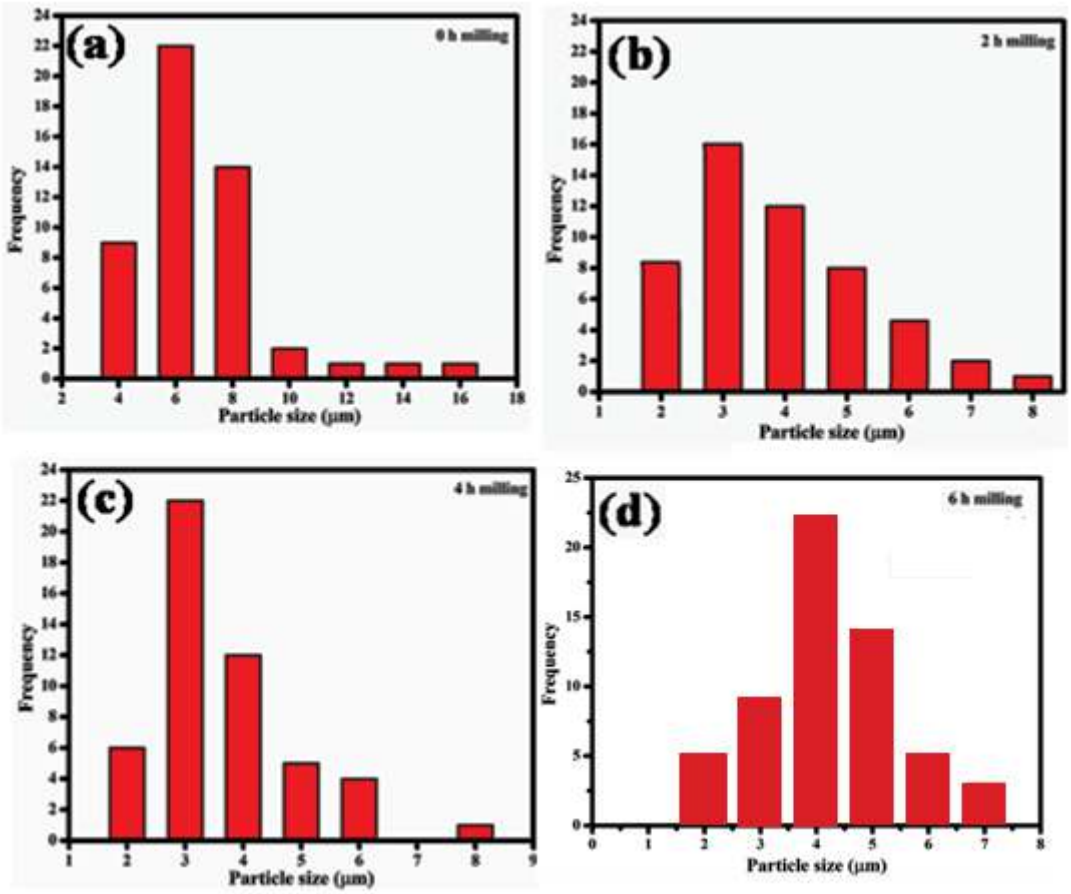

Fig. 4.7: Particle size distribution of Cu4Ni-4TiC composite powders as a function of the milling times (a) 0 h, (b) 2 h, (c) 4 h and (d) 6 h.

The milled powder was subjected to EDS analysis to confirm that mechanical alloying did not produce any foreign element. Figure 4.8 shows the EDS spectra of Cu4Ni-4TiC powder milled for 6 h. No foreign element has been detected by the EDS analysis as evident from Fig. 4.8.

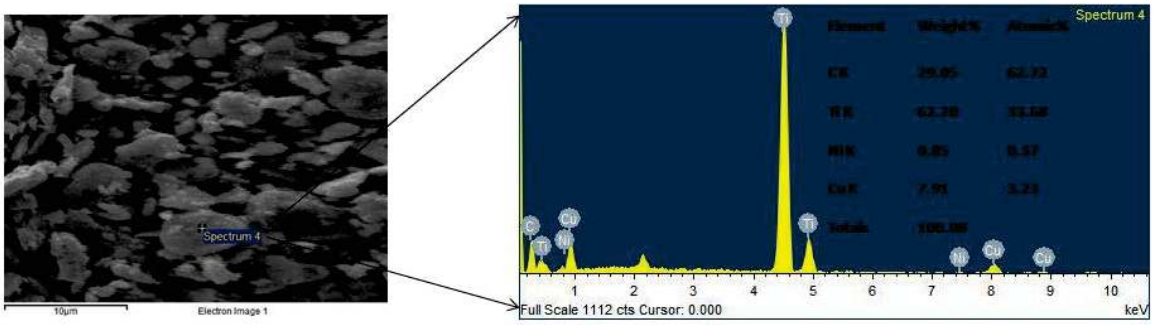

Fig.4.8: The EDS spectra of Cu4Ni-4TiC composite powder milled for 6 h.

The XRD patterns of Cu4Ni-x wt.% TiC (x = 2, 4, 6 and 8) composite after 6 h of mechanical alloying are shown in Fig. 4.9. The diffraction patterns show the presence of peaks corresponding to Cu, Ni and TiC indexed by using JCPDS file and the same have been marked on the diffraction pattern. Cu, TiC and Ni peaks were indexed using JCPDS file numbers 85–1326, 89–3828 and 04–0850, respectively. The peaks corresponding to TiC are observed to become a bit sharper with increasing wt.% of TiC. Further, Fig. 4.10 shows the XRD patterns of Cu4Ni-4wt.%TiC composite powders after 0, 2, 4 and 6 h of mechanical alloying. One could also observe the peaks corresponding to Cu, Ni and TiC. However, the broadening of peaks corresponding to Cu is observed to occur with increasing time of milling time for a particular amount of addition of TiC.

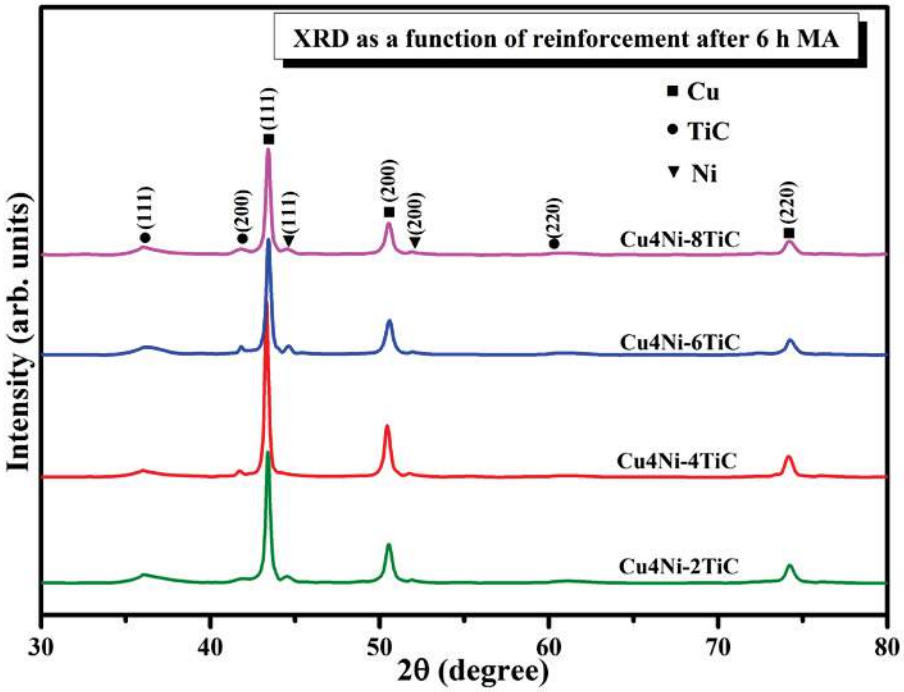

Fig.4.9: XRD patterns of Cu4Ni–x wt. % TiC composite powders after 6 h MA.

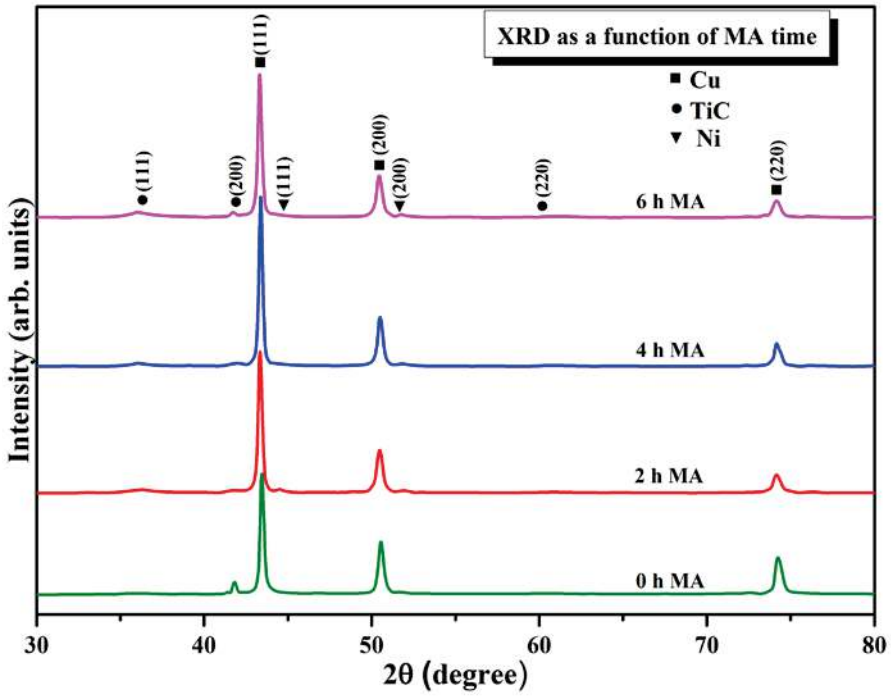

Fig.4.10: XRD patterns of Cu4Ni–4TiC composite powders after 0, 2, 4 and 6 h of MA.

Table 4.1 shows the crystallite size, lattice strain and lattice parameter of Cu4Ni-x wt.% TiC (x =0, 2, 4, 6, and, 8 wt.%) composite powders. The crystallite size of Cu4Ni matrix alloy is 83 *nm*, which decreases to 74 *nm* with the addition of 2 wt.% TiC. The crystallite size further reduces to 44 *nm* with the addition of 4 wt. %.TiC. However, crystallite size increases from 46 *nm* to 112 *nm* as TiC content increases from 6 to 8 wt.%. The definite lattice parameter was obtained by constructing a linear plot between lattice parameter calculated for each Bragg's angle and the corresponding value of $\cos^2\theta/\sin\theta$ and lattice parameters are given in Table 4.1

Table 4.2 presents the effect of milling time on the structural properties in terms of crystallite size, lattice strain and lattice parameter of Cu4Ni-4TiC composite powder. It is observed that crystallite size decreased to 31 *nm* for mechanical alloying obtained by 2 h milling and after that it increases. It becomes 44 *nm* for 6 h milling. The definite lattice parameter was obtained by constructing a linear plot between lattice parameter calculated for each Bragg's angle and the corresponding value of $\cos^2\theta/\sin\theta$.

Table 4.1 Structural characterization of Cu4Ni-x wt.% TiC composite powder after 6 h of milling time, x = 0, 2, 4, 6 and 8 wt.%.

S. No.	Composition	Crystallite size (t), nm	Lattice strain (ε), %	Lattice parameter (a), Å
1	Cu4Ni	83	0.214 ± 0.002	3.617 ± 0.096
2	Cu4Ni-2TiC	74	0.188 ± 0.002	3.615 ± 0.001
3	Cu4Ni-4TiC	44	0.062 ± 0.001	3.613 ± 0.001
4	Cu4Ni-6TiC	46	0.134 ± 0.003	3.616 ± 0.004
5	Cu4Ni-8TiC	112	0.377 ± 0.001	3.616 ± 0.003

Table 4.2 Structural characterization of Cu4Ni-4TiC composite powder after 6 h of milling time.

Milling time, H	Crystallite size (t), Nm	Lattice strain(ε), %	Lattice parameter (a), Å
0	48	0.019 ± 0.002	3.608 ± 0.008
2	31	0.075 ± 0.002	3.614 ± 0.005
4	38	0.066 ± 0.001	3.615 ± 0.003
6	44	0.062 ± 0.002	3.613 ± 0.002

It can be seen from Table 4.2 that the crystallite size is minimum for 2 h of milling time, which may provide a relatively higher hardness to the composite in comparison to other milling times if one goes by the fact that hardness increases with decreasing size of crystallite. Therefore, one may conclude that 2 h is the optimum milling time for attaining a relatively harder composite.

4.1.2 Compressibility behavior

The compressibility curves of Cu4Ni-4TiC composite processed for various times and compacted at different pressures are shown in Fig.4.11. The curves demonstrate a distinctive compressibility performance for milled metallic powders. It is observed that

the green density of the compacts changes with increasing milling time depending on the compaction pressure. The composite powder milled for a longer duration is found to possess a relatively higher green density when compacted at the lowest pressure of 250 MPa used in the present study as shown in Fig. 4.11. However, the trend gets reversed as the compaction pressure is increased to 850 MPa at which the powder milled for 0 h has the largest relative density and the one milled for 6 h has the lowest as evident from Fig. 4.11.

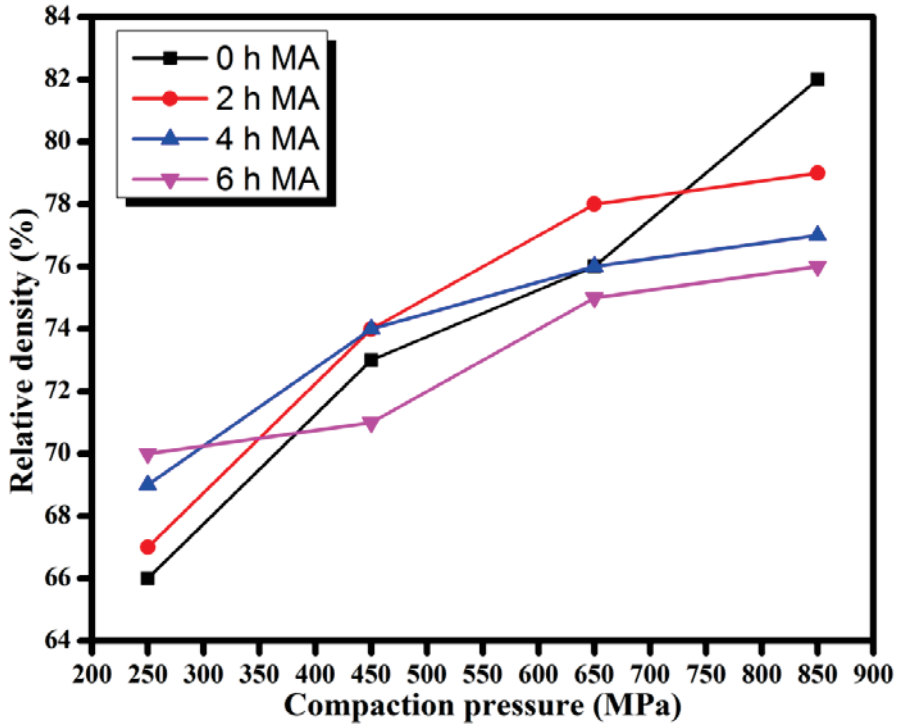

Fig 4.11: Compressibility curves of Cu4Ni-4TiC composite powder at different compaction pressure.

Several compaction equations have been proposed earlier for modeling the relationship between powder density and porosity with the compaction pressure. The compaction equations are useful for analyzing the effect of particle rearrangement at low pressure and plastic deformation at high pressure. In the present investigation, Panelli and Ambrosio Filho (Panelli et al., 2001), Heckel (Heckel, 1961), and Ge (Ge, 1991) compaction equations have been used to assess the role of hard TiC particles on the compressibility

behavior of Cu4Ni matrix alloy powder. Equations (4.1), (4.2) and (4.3), respectively, show the Panelli and Ambrosio Filho, Heckel, and Ge compaction equations.

$$\ln\left(\frac{1}{1-\mathrm{D}}\right) = \mathrm{A}\sqrt{\mathrm{P}} + \mathrm{B} \tag{4.1}$$

$$\ln\left(\frac{1}{1-\mathrm{D}}\right) = \mathrm{AP} + \mathrm{B} \tag{4.2}$$

$$\log\left[\ln\left(\frac{1}{1-\mathrm{D}}\right)\right] = \mathrm{A}\log\mathrm{P} + \mathrm{B} \tag{4.3}$$

Where, D is the relative density of the compacted material and P is the applied pressure. A and B are constants. A linear plot can be constructed for the values of $\ln\left(\frac{1}{1-\mathrm{D}}\right)$ as a function of $\sqrt{\mathrm{P}}$ in Panelli and Ambrosio Filho's equation (4.1) (Panelli et al. 2001), $\ln\left(\frac{1}{1-\mathrm{D}}\right)$ as a function of P in Heckel's equation (4.2) (Heckel, 1961) and $\log\left[\ln\left(\frac{1}{1-\mathrm{D}}\right)\right]$ as a function of log (P) in Ge's (4.3) (Ge, 1991) equation. Parameter A, the slope of the linear plots, signifies the ability of the powder to get plastically deformed during compaction. Higher A values correspond to soft metals such as aluminum or copper whereas lower A values correspond to hard powders, like ceramics. The parameter B, the intercept of the linear plots at zero pressure, expresses the apparent density of the compacts without application of pressure (Gan et al., 2008).

Figures 4.12 (a) to (c) show the compressibility curves for Cu4Ni-4TiC composite powder plotted using Eqs. (4.1), (4.2) and (4.3) and the values of parameter A and coefficient of correlation (R^2) are given in Table 4.3. The data have been fitted by linear least square method. All the curves illustrated in Figs. 4.12 (a) through (c) show a linear variation with coefficient of correlation, R^2, very close to unity as evident from Table 4.3, indicating that the Eqs. (4.1), (4.2) and (4.3) are obeyed well.

In the present investigation, Panelli and Ambrosio Filho equation has been used to understand the plastic deformation capacity of the composite powder with ball milling duration. Parameter A plays very important role in the compaction equation and it

denotes the plastic deformation capacity of the powder during compaction. It is evident from Table 4.3 that as the milling duration increases, parameter A decreases from 0.0397 to 0.0222 while using the Panelli and Ambrosio Filho equation. The value of A decreases from 0.0009 to 0.0005 if one considers the Heckel equation (4.2) whereas it decreases from 0.3301 to 0.0005 for Ge equation (4.3). It indicates that the increasing duration of milling reduces the capacity of the powder to get deformed plastically.

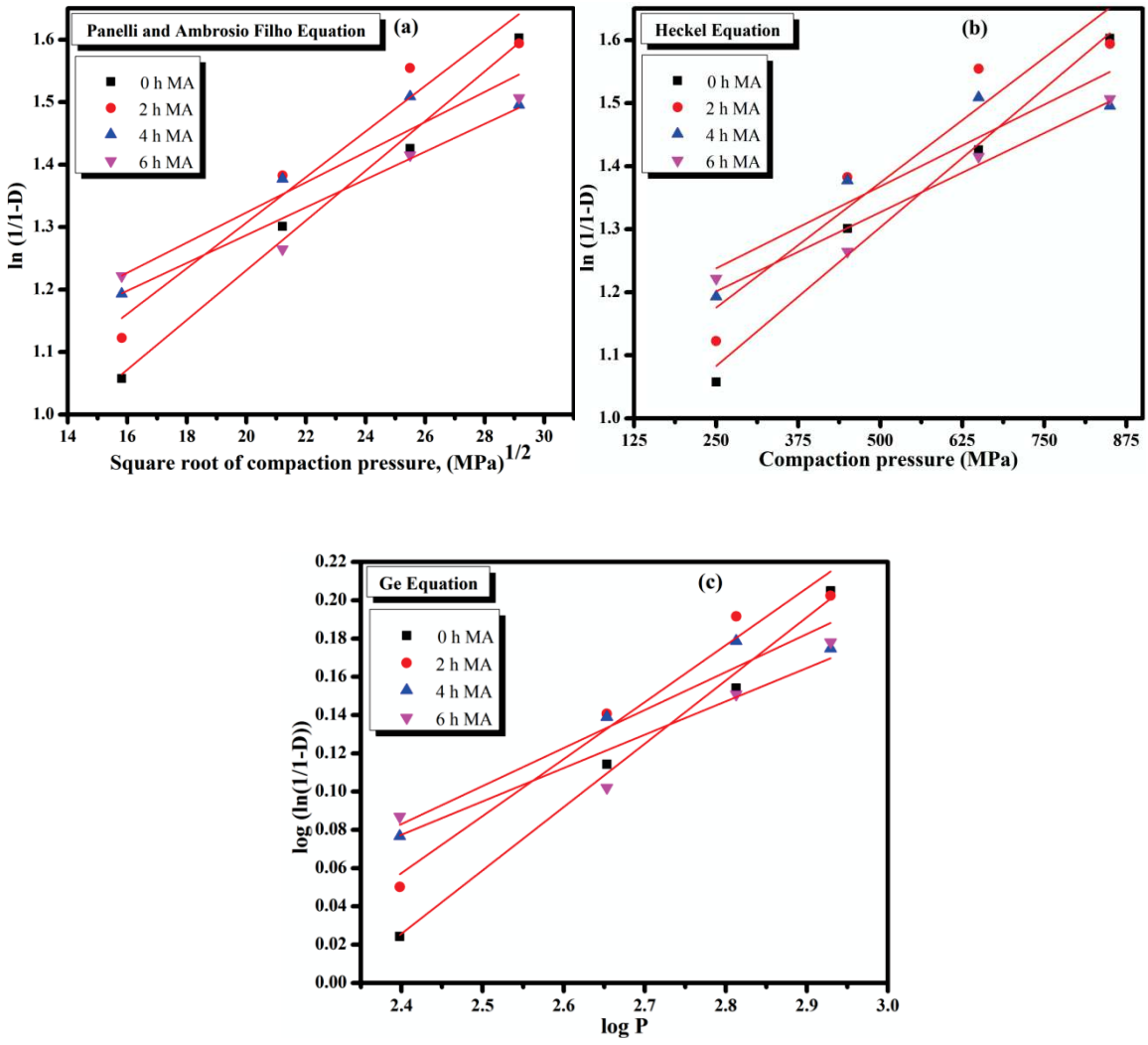

Fig.4.12: Compressibility curve of experimental data of Cu4Ni-4TiC composite powder fitted by (a) Panelli and Ambrosio Filho, (b) Heckel and (c) Ge's compaction equations.

Table 4.3 The Parameter (A), correlation coefficient (R^2) values of Cu4Ni-4TiC composite powders at different milling times using various compaction equations.

Sr. No.	Milling time (h)	Panelli		Heckel		Ge	
		A	R^2	A	R^2	A	R^2
1	0	0.0397	0.99	0.0009	0.99	0.3301	0.99
2	2	0.0364	0.97	0.0008	0.95	0.2972	0.98
3	4	0.0241	0.95	0.0006	0.94	0.1982	0.96
4	6	0.0222	0.97	0.0005	0.98	0.0005	0.98

4.1.3 Microstructure

4.1.3.1 Optical Microscopy

Figure 4.13 shows the optical microstructure of all the materials used in present investigation at 100X. Figure 4.13 (a) shows the microstructure of Cu4Ni alloy where nickel is observed to be well dispersed in the copper as marked by arrow. Some pores, denoted by round circles can also be observed in the micrograph. Formation of pores is an inherent properly of powder metallurgy technique and cannot be avoided totally. Figures 4.13 (b) through (e) present the microstructures of Cu4Ni-2TiC, Cu4Ni-4TiC, Cu4Ni-6TiC and Cu4Ni-8TiC, respectively. One may observe almost homogeneous distribution of TiC particles (marked by arrows) in the matrix in all these micrographs. However, the amount of TiC particles is also observed to increase with increasing amount of TiC from 2 to 8 wt.% as one moves from Fig. 4.13 (b) to 4.13 (e).

4.1.3.2 Scanning electron microscopy

Figures 4.14 (a) to (e) show the SEM micrographs of Cu4Ni matrix alloy and Cu4Ni-2TiC, Cu4Ni-4TiC, Cu4Ni-6TiC and Cu4Ni-8TiC composites developed in the

present study via high energy ball milling followed by compaction and sintering. The micrographs show the distinguished phases as light grey, white, dark grey areas and sharp edged particles, representing respectively, copper, nickel, porosity, TiC. The various phases have been marked on the micrographs by arrows. Titanium carbide particles (TiC) appear to be distributed uniformly in the matrix alloy as could be observed in Figs. 4.14 (b) to (e).

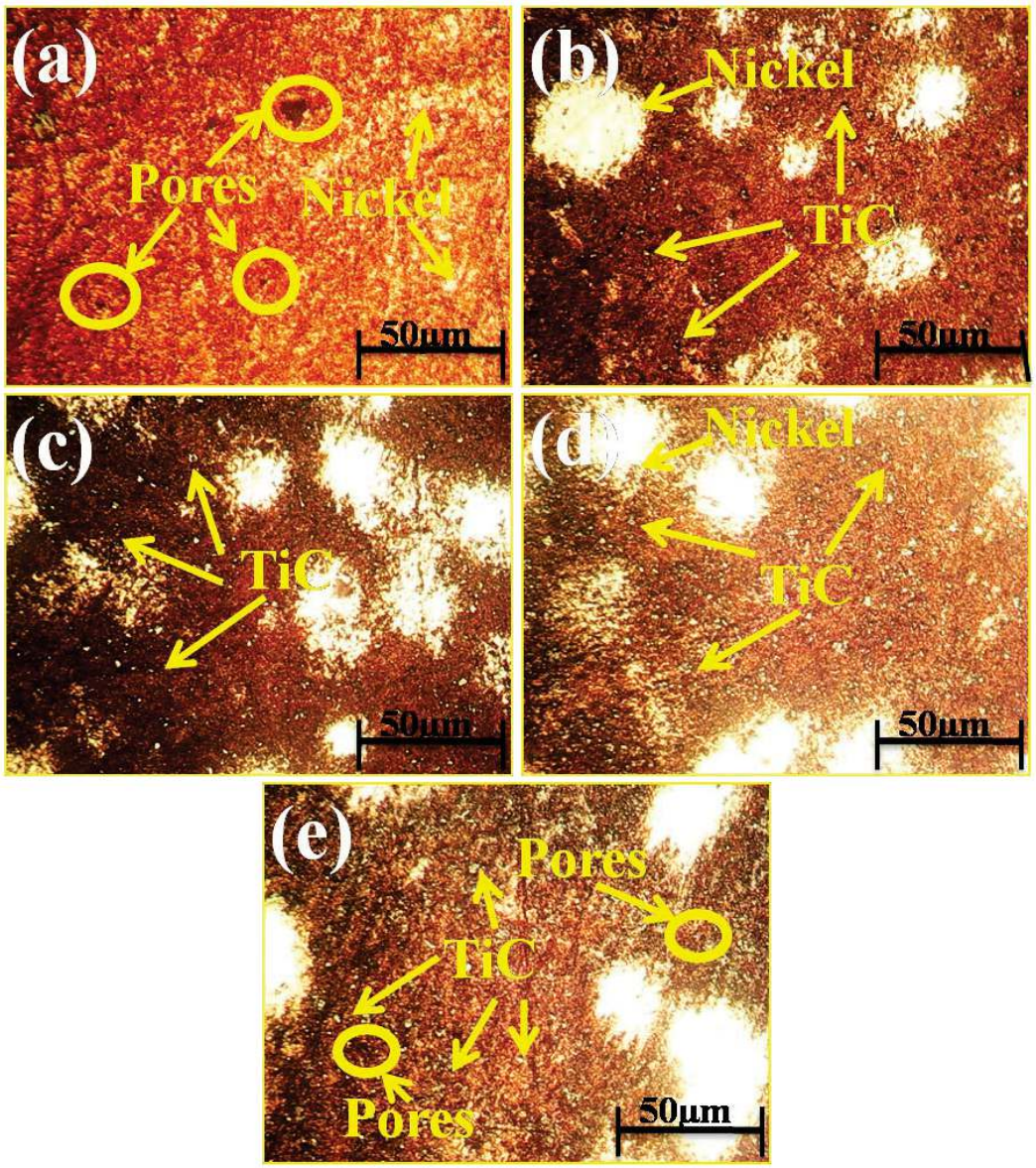

Fig 4.13: Optical micrographs of sintered materials after 2 h milling showing microstructure of (a) Cu4Ni, (b) Cu4Ni-2TiC, (c) Cu4Ni-4TiC, (d) Cu4Ni-6TiC and (e) Cu4Ni-8TiC.

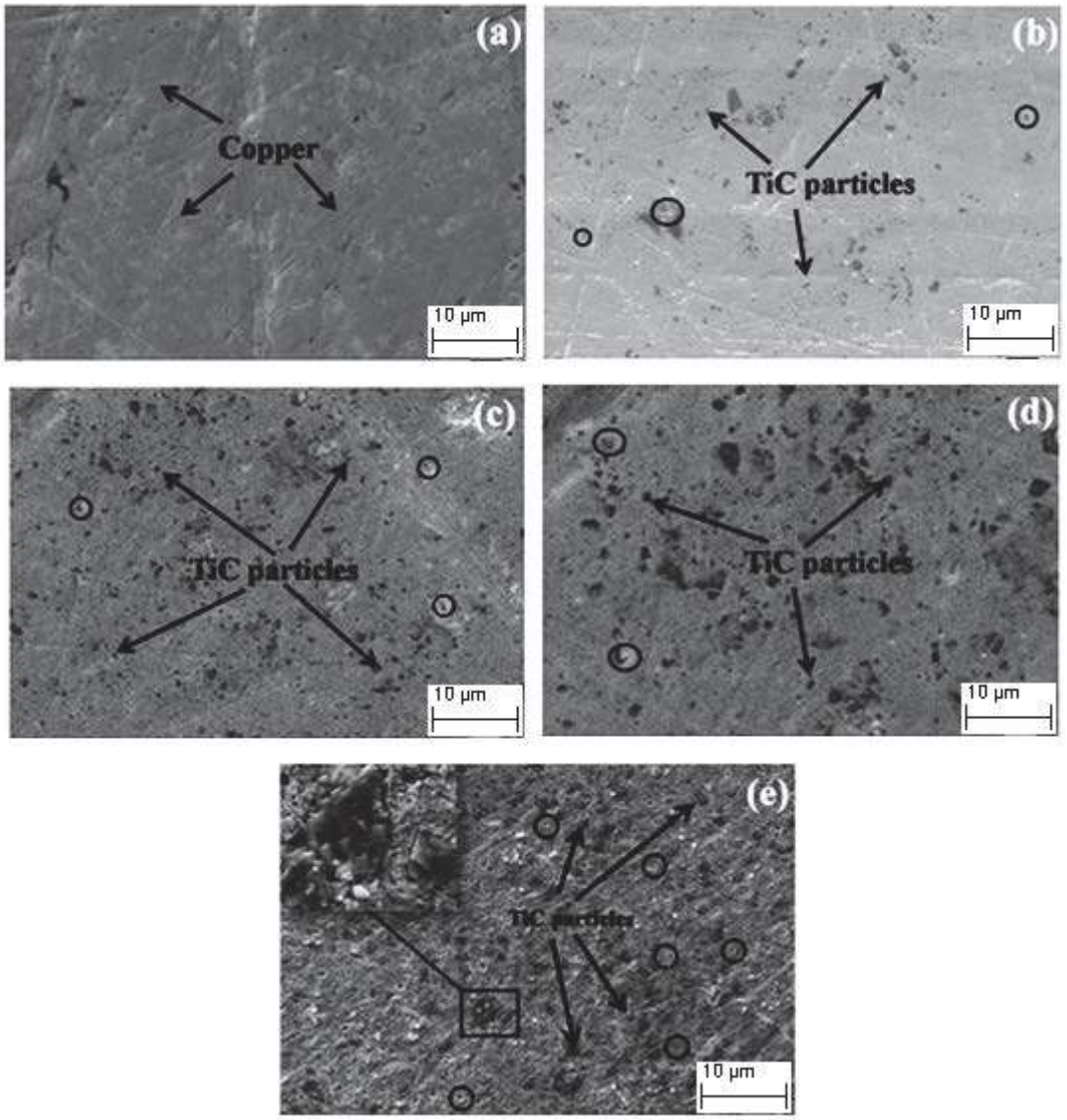

Fig 4.14: SEM micrographs of (a) Cu4Ni matrix alloy, (b) Cu4Ni-2TiC, (c) Cu4Ni-4TiC, (d) Cu4Ni-6TiC and (e) Cu4Ni-8TiC.

EDS analyses of the marked region of Cu4Ni alloy, Cu4Ni-4TiC and Cu4Ni-8TiC composites, given in Figures 4.15 (a) to (c) shows the presence of corresponding elements in the respective composites.

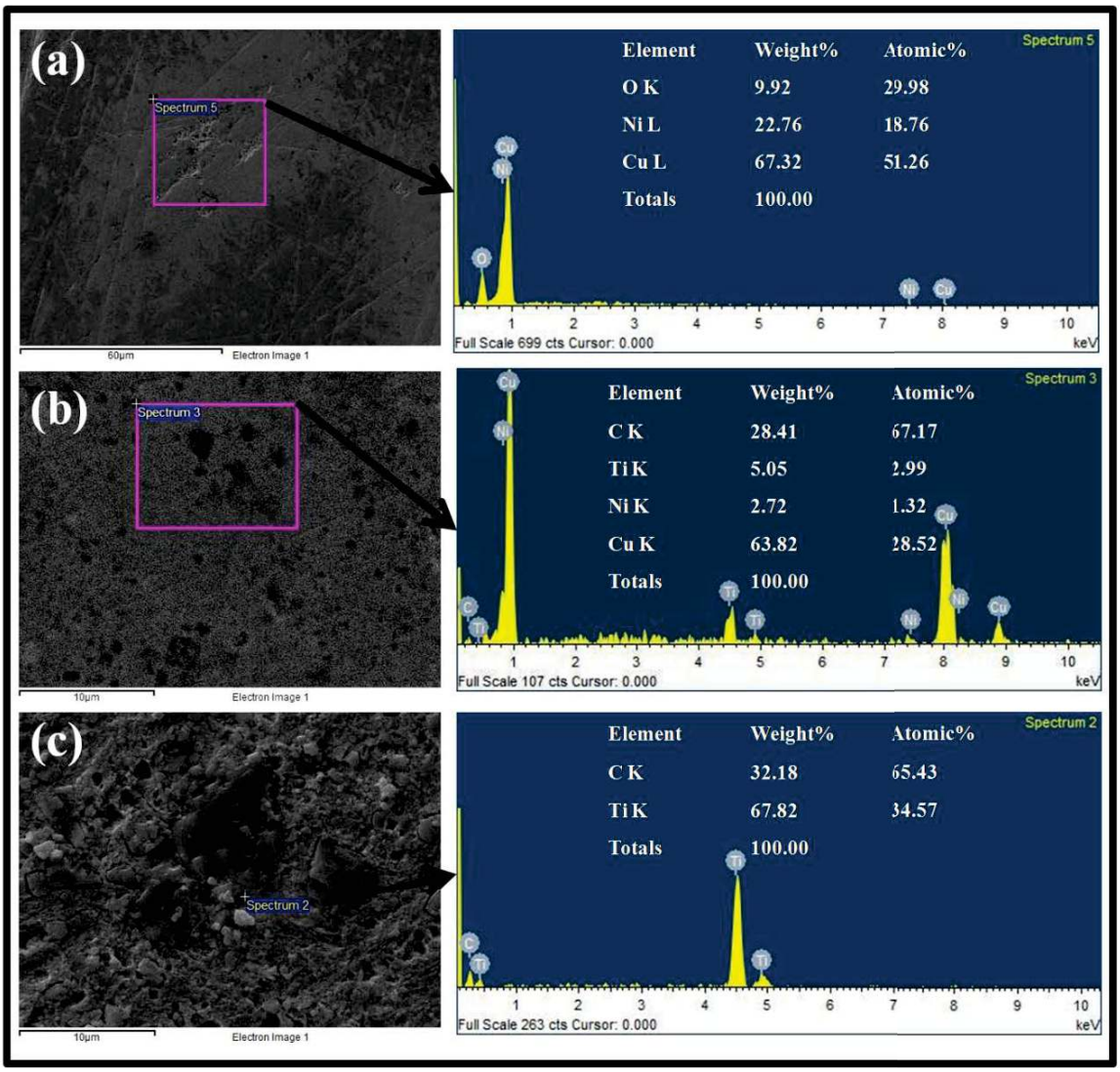

Fig.4.15: EDS analyses of (a) Cu4Ni alloy, (b) Cu4Ni-4TiC and (c) Cu4Ni-8TiC.

Figures 4.16 (a) through (c) show the HR-SEM micrographs of Cu4Ni alloy, Cu4Ni-4TiC and Cu4Ni-8TiC whereas Fig. 4.16 (d) shows the EDS analysis of Cu4Ni-4TiC composite. Figure 4.16 (a) shows the presence of copper-nickel matrix alloy along with some pores as marked by arrows. The presence of TiC particles which appear to be distributed homogeneously throughout the matrix could be seen in Fig. 4.16 (b). The homogeneous dispersion of TiC particles is supposed to be necessary for the improved mechanical properties. Some agglomeration of TiC particles and matrix alloy takes place with increasing amount of TiC as evident from Fig. 4.16 (c) which corresponds to Cu4Ni-8TiC. These agglomerates have deleterious effect on the density and hardness.

EDS spectrum of Cu4Ni-4TiC composite given in Fig. 4.16 (d) confirms the presence of TiC.

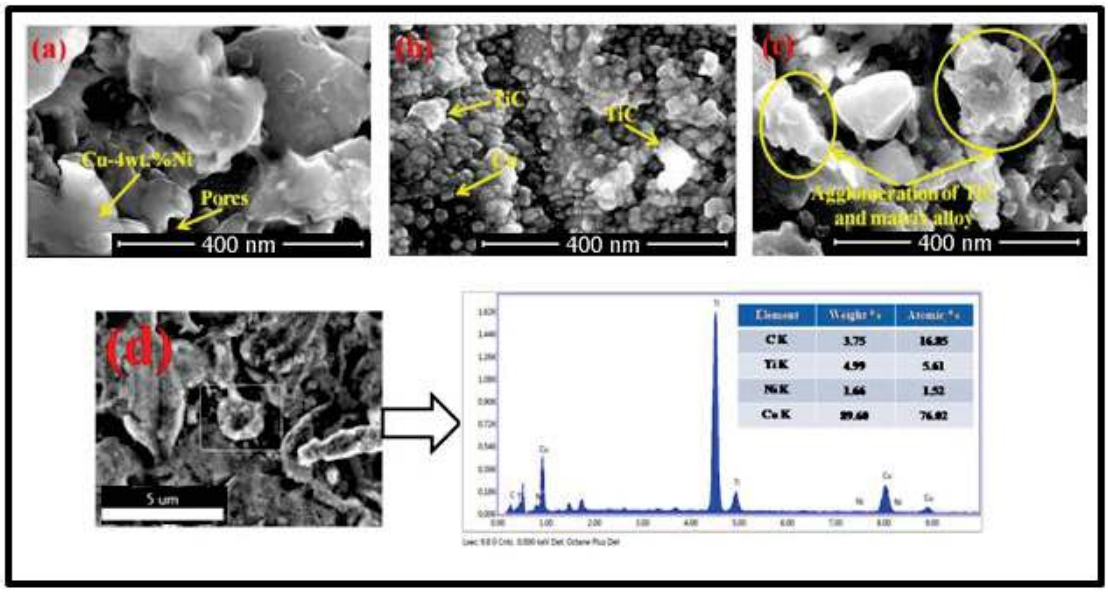

Fig.4.16: HR-SEM micrograph of (a) Cu4Ni, (b) Cu4Ni-4TiC, (c) Cu4Ni-8TiC and (d) EDS analysis of Cu4Ni-4TiC composite.

4.1.4 XRD analysis

Figure 4.17 shows the X-ray diffraction (XRD) patterns of the matrix alloy and TiC reinforced composites after sintering at 850^{o}C for 1 hour holding time. Diffraction peaks present in the specimen are matched with the XRD-JCPDS files of different compounds. One could observe the peaks corresponding to Cu-Ni and TiC only in the composites indicating that either no intermetallic compounds were formed between Cu-Ni and TiC during sintering or if at all formed, the amount might have been below the detection limit of X ray.

4.1.5 Density measurement

The green compacts have been sintered at a certain temperature and holding time to increase the density. To achieve the better densification of the compacted specimens it is necessary to first optimize the sintering temperature. For the sake of optimization

purpose, the Cu4Ni-4TiC compacted specimens were sintered at three temperatures i.e., 800, 850 and 900°C. Table 4.4 gives the relative density and sintered density of Cu4Ni-4TiC composite at different sintering temperatures and milling time.

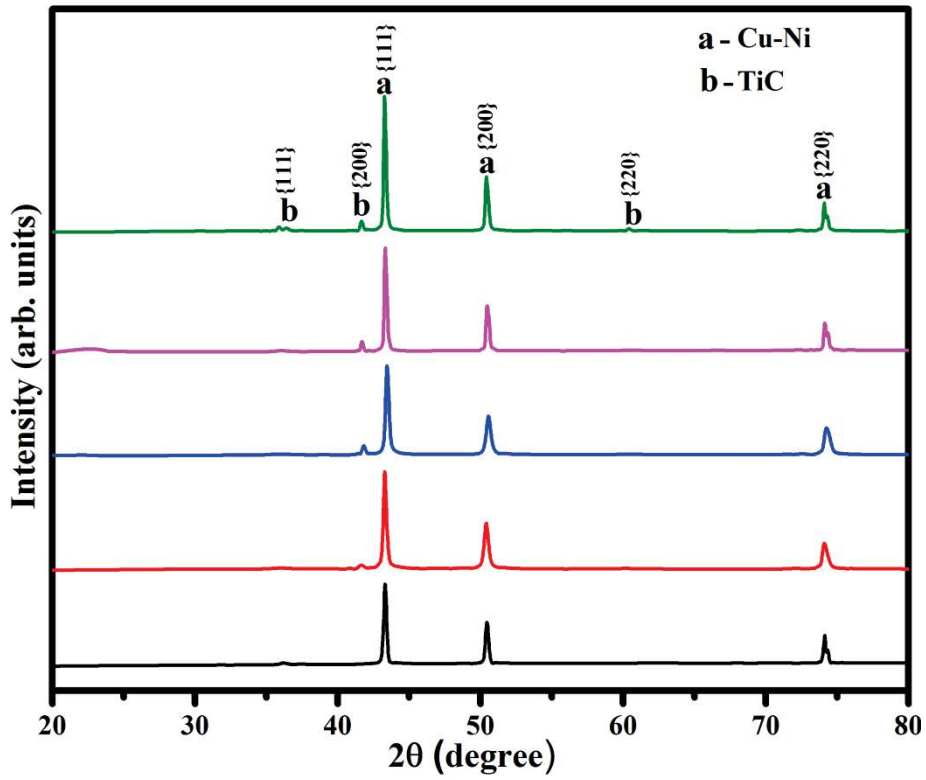

Fig.4.17: XRD patterns of Cu4Ni–x wt. % TiC (x = 0, 2, 4, 6 and 8) composites sintered at 850°C.

It can be seen from the Table 4.4 that maximum densification (90.81%) is achieved at 850°C. It is also evident from Table 4.4, that the relative density is maximum for 2 h milling and decreases thereafter with longer milling times. Hence, milling duration of 2 h and sintering temperature of 850°C have been used in the present investigation for synthesizing the composites.

Table 4.5 presents the effect of addition of TiC particles on the densification of the matrix alloy at 850°C. The maximum density has been observed for Cu4Ni-4TiC composite. The relative density has also been found to increase with increasing addition of TiC to 4 wt.% beyond which it starts decreasing as the TiC content is raised to 6 and 8 wt.% as evident from Table 4.5.

Table 4.4 Relative density and sintered density of Cu4Ni-4TiC composite at different sintering temperatures and milling times.

Milling time (h)	800°C		850°C		900°C	
	Relative density (%)	Sintered density ($kg/m^3 \times 10^3$)	Relative density (%)	Sintered density ($kg/m^3 \times 10^3$)	Relative density (%)	Sintered density ($kg/m^3 \times 10^3$)
0	85.13 ±0.14	7.47 ± 0.10	88.95 ± 0.18	7.82 ± 0.05	88.11 ± 0.19	7.72 ± 0.06
2	85.99 ± 0.12	7.54 ± 0.09	90.81 ± 0.17	7.96 ± 0.05	88.38 ±0.16	7.75 ± 0.08
4	81.77 ± 0.15	7.17 ± 0.06	88.38 ± 0.12	7.75 ± 0.07	83.71 ±0.19	7.34 ± 0.04
6	77.21 ± 0.19	6.77 ± 0.07	84.39 ± 0.16	7.46 ± 0.08	76.41 ± 0.17	6.72 ± 0.06

Table 4.5 Relative density and sintered density of composites 850°C for 2 h milling duration.

S.No.	Specimen designation	Relative density (%)	Sintered density ($kg/m^3 \times 10^3$)
1	Cu4Ni	86.31 ± 0.19	7.70 ± 0.08
2	Cu4Ni-2TiC	88.81 ± 0.15	7.86 ± 0.06
3	Cu4Ni-4TiC	90.81 ± 0.17	7.96 ± 0.05
4	Cu4Ni-6TiC	85.35 ± 0.18	7.42 ± 0.09
5	Cu4Ni-8TiC	81.44 ± 0.12	7.01 ± 0.05

4.1.6 Hardness measurement

Figure 4.18 depicts the variation of micro hardness of Cu4Ni-4TiC composites with milling time, at three different sintering temperatures of 800, 850 and 900°C. It is observed that micro-hardness behavior is dependent on the density of the composite. At

800°C the hardness values are 76, 82, 80 and 62 HV whereas the same at 850°C are 96, 109, 97 and 67 HV. The micro-hardness values obtained at 900°C are 79, 87, 75 and 64 HV, respectively. It can also be observed that maximum micro-hardness of 109 HV is obtained for the milling time of 2 h and 850°C. It is also apparent from Table 2 that minimum crystallite size (31 *nm*) is obtained for 2 h milling duration and after which it increases which ultimately affects the micro-hardness as stated earlier also. Figure 4.19 shows the variation of micro-hardness of the composites with wt.% of TiC.

The micro-hardness of the composites, namely, Cu4Ni, Cu4Ni-2TiC, Cu4Ni-4TiC, Cu4Ni-6TiC and Cu4Ni-8TiC are 60, 75, 109, 90 and 77 HV, respectively. One could observe that the micro-hardness increases with increasing amount of TiC till 4 wt.% beyond which it starts decreasing as evident from Fig. 4.19. The micro-hardness increases from 60 HV to 109 HV with an addition of 4 wt.% TiC which is almost 82% more than the matrix alloy. However, the micro-hardness decreases to 90 HV with the addition of 6 wt.% TiC. Still, further reduction in micro-hardness to 77 HV is also observed with the addition of 8 wt. % TiC, the highest amount added in the present study probably due to the agglomeration of TiC.

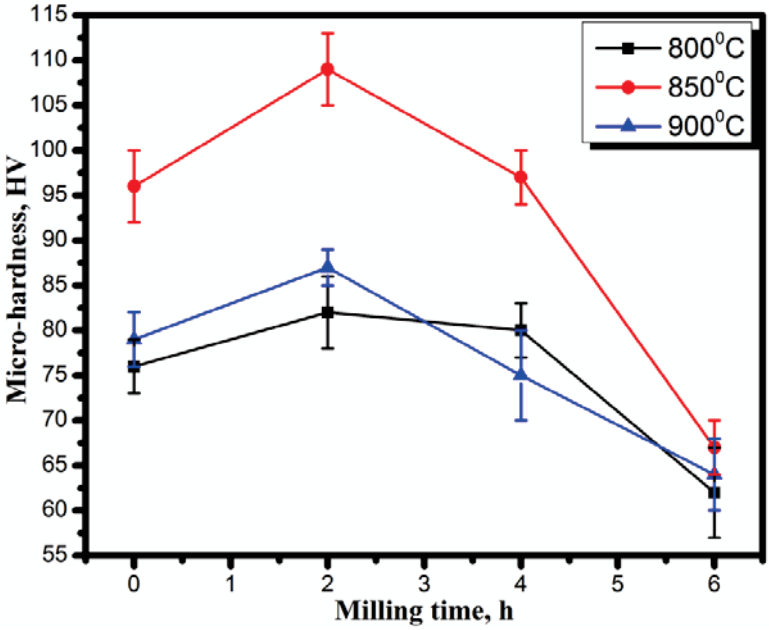

4.18: Micro-hardness of Cu4Ni-4TiC composite with milling time.

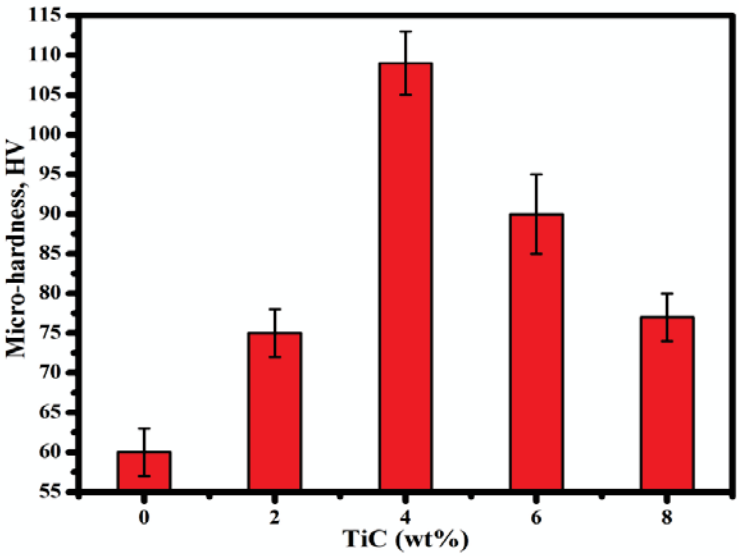

Fig.4.19: Variation of micro-hardness of composites with TiC content.

4.1.7 Electrical resistivity measurement

Figure 4.20 shows the variation of electrical resistivity of Cu4Ni matrix alloy and other composites synthesized in the present study. The electrical resistivity is found to increase with increasing TiC content as observed from Fig. 4.20. The measured values of resistivity for Cu4Ni, Cu4Ni-2TiC, Cu4Ni-4TiC, Cu4Ni-6TiC and Cu4Ni-8TiC are 3.65×10^{-8}, 5.84×10^{-8}, 6.07×10^{-8}, 6.4×10^{-8} and 6.85×10^{-8} Ω-m, respectively.

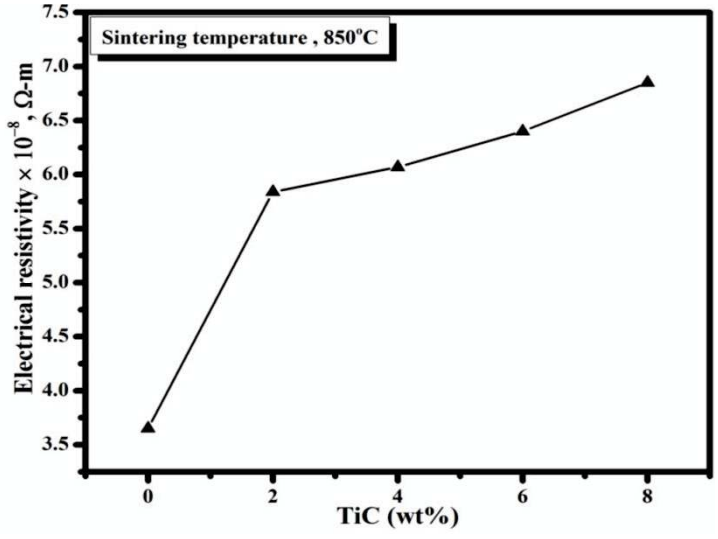

Fig.4.20: Variation of electrical resistivity with TiC content.

4.2 DISCUSSION

The powders of Cu, Ni and TiC powders having dendritic, spherical and sharp-edged morphologies as shown in Figs. 4.1, 4.2 and 4.3, respectively, have been mixed using a high energy ball mill to synthesize the composites following conventional compaction and sintering route. The metal powders are soft in nature and high energy ball milling deforms the particles and changes their morphology. Further, the welding of the flattened particles promotes the formation of agglomerates as shown in Fig. 4.4 (a). The particle size has been observed to decrease with increasing TiC content up to 4 wt.% which could be observed from Figs. 4.4 (a) to (c) showing the morphology of particles milled for 6 h duration and Figs. 4.5 (a) to (c) representing the particle size distribution for Cu4Ni, Cu4Ni2TiC and Cu4Ni4TiC, respectively. However, the particle size is found to increase for the TiC addition beyond 4 wt.% i.e., for addition of 6 and 8 wt. % as evident from a comparison of Figs. 4.4 (c), (d) and (e) and Figs. 4.5 (c), (d), (e). It is clear from the histogram that particle size of the matrix alloys are in the range of 6-20 μm whereas the particle size of the 4 wt.% TiC reinforced composites are in the range of 4-5 μm. A decrease in particle size due to the reinforcement of TiC particles upto 4 wt. % into the matrix alloy may be attributed to the fact that reinforced TiC particles function as a milling agent besides other milling media (disc and vial speed, BPR, balls, etc.) and cause severe plastic deformation of the powder particles as indicated by Kamrani et al. (2007) also. Another reason for the decrease in particle size could be the refining of the matrix alloy caused by the increasing amount of TiC particles during mechanical alloying process as suggested by Jeyasimman et al. (2014). However, one could observe an increase in particle with the increase in TiC content beyond 4 wt.% as indicated in the micrographs shown in Figs. 4.4 (d) and (e). This may be attributed to the tendency of TiC ceramic particles to form agglomerates in the matrix alloy. A similar trend of the decrease in particle size with increasing amount of TiC has also been reported by Jeyasimman et al. (2014) for Al 6016 composites reinforced by TiC particles. During ball milling the constituent powders experience high-energy collisions repeatedly which lead to plastic deformation, cold welding and fracture of the powder particles. The cold welding process is believed to increase the powder particle size whereas fracturing causes a reduction the particle size of the powders (Suryanarayana, 2001).

In order to understand the effect of milling duration on the shape of milled powders, typical morphologies of Cu4Ni-4TiC composite powder milled for 0, 2, 4 and 6 h have been analyzed. Cu-4wt.%Ni-4wt.% TiC powders were blended for 8 h at a rotational speed of 0.66 s^{-1} and this has been regarded as 0 h duration of the mechanically milling as mentioned above. Further these composite powders were high energy milled/mechanically alloyed (MA) for 2, 4 and 6 h, respectively at a speed of 400 rpm. Figs. 4.6 (a) through (d) show the morphologies corresponding to 0, 2, 4 and 6 h duration of milling. Figure 4.6 (a) shows that particle have a flaky shape which changes to almost equiaxed after 6 h of milling as represented in Fig. 4.6 (d). During early stage of milling TiC particles stick to the Cu-Ni powders and get cold welded with them leading to entrapment of TiC particles within the matrix alloy powder. The entrapped TiC particles being brittle provide easy path for crack propagation in Cu-Ni matrix under cyclic loading during high energy ball milling and cause fracture of the matrix. Also, during milling the powders undergo cold working which intensifies the initiation and propagation of cracks within powder particles. These cracks would propagate through the matrix alloy and finally fracture the Cu particles. These fresh fractured surfaces with TiC particles sticking on them, would weld with other surfaces. The process of repeated fracture and cold welding ensures the uniform distribution of TiC within the Cu-Ni matrix through the mechanism explained earlier by Khakbiz et al. (2009). As the milling duration is enlarged to 2 h, the particles collide with each other and plastic deformation takes place. Cold welding is a dominant cause for the increase in particle size during this period and particles become flattened as shown in Fig. 4.6 (b). With the increasing milling time the fragmentation of cold welded powders occurs due to repeated fracture resulting in a decrease in particle size as evident from Fig. 4.6 (c) which corresponds to 4 h of mechanical alloying (MA). A further increase in milling duration leads to domination of fracturing process resulting in a decline in particle size upto a limit where a balance is reached between cold welding and fracturing. The particles become equiaxed after 6 h MA as seen from Fig. 4.6 (d). The reduction in size of particles with increased duration of milling could be easily seen from the histograms shown in Fig. 4.7. The minimum particle size of the composite powders for the 6 h milling time is found to be 1-4.5 μm.

It is evident from the spectrum that Cu, Ni, Ti, and C peaks are present in the powder as shown in Fig. 4.8. This ensures that powder did not contain any extra element due to contamination from the milling media (milling vials and balls). XRD spectrums given in Figs. 4.9 and 4.10 also reflect the presence of only those components which are added to synthesize the composite. The formation of intermetallic compound may take place between the constituent elements during processing but no intemetallic compound could be detected by XRD in the present investigation. Hence, one may conclude that either no intermetallic compound was formed or if at all formed it was below the detection limit of XRD. It is observed from Fig 4.10 that Cu peak intensity decreases whereas peak width increases and this may be attributed to the structural refinement caused by the mechanical alloying. Similar observations of broadening of peaks after milling process have been reported by Akbarpour et al. (2014).

Table 4.1 depicts the variation of some structural parameters with respect to increasing amount of TiC after a fixed milling duration of 6 h. Initial decrease in the crystallite size as seen from Table 4.1 can be attributed to the presence of hard TiC particles in the matrix alloy powder which produce severe plastic deformation and act as a milling agent, promoting thus the fracturing of the matrix alloy with a consequent reduction in crystallite size. Kamrani et al. (2007) also reported that hard ceramic particles perform as a milling agent and result in fracturing of relatively softer matrix leading to reduction in crystallite size. It is also observed from Table 4.1 that after a certain extent of reinforcement (4 wt.%) the crystallite size increases. The possible reason can be that when the TiC particles increases after 4 wt.% the agglomeration takes place as observed in SEM images (Fig. 4.4). These agglomerates spread on the surface of the matrix particles and generate a network of inclusions which not only affects the plastic deformation of powders but also hinders the welding process as suggested by Hesabi et al., (2006). No certain trend with regard to change in lattice strain could be observed. The abrupt change in lattice strain may be attributed to the increased lattice defects and dislocation density caused by the reinforced TiC particles and the other milling media (balls, BPR, vial and disc speed, etc.) used during milling. There is no change in lattice parameter with the addition and/ or increase of TiC amount.

The variation of structural parameters with respect to milling time for a fixed amount of TiC is reported in Table 4.2. The reason for the decline in crystallite size can be attributed to the presence of TiC particles during the milling as well as the balls in the ball milling. The TiC particles are very hard in nature and it may create plastic deformation with the help of the milling balls and thus crystallite size decreases [Hesabi, Z. R., et al. (2006)]. It is also observed that crystallite size increases after a certain milling time. The possible reason for the increase in crystallite size can be credited to the fact that after a certain interval of milling the heat energy is generated due to the milling action and this heat energy can cause fast grain boundary diffusion that acts as an annealing effect which in turn leads to an increase in the crystallite size [Elshimy. H., et al. (2014)].

Prolonged milling enhances the work hardening effect of the powder particles. The increase in the lattice strain can be credited to the plastic deformation caused by high energy ball milling. It was reported in case of Cu-TiC composite system that the rate of straining is directly interrelated to the severity of plastic deformation experienced by the metallic matrix during milling as suggested by Rathod et al. (2013). It can be seen from the Table 4.2 that lattice strain decreases after 2 h of milling period which is also related to the crystallite size as discussed earlier. The decrease in the lattice strain can be caused by the softening of the grain boundary which has also been reported earlier by Sivasankaran et al. (2010). Slight changes in the lattice parameter may be attributed to the existence of vacancies, dissolution of minor elements and influence of milling agents as suggested by Saravanan et al. (2015).

Both the morphology of particles obtained after milling and the hardness of the particles shall be considered for explaining the compressibility behavior of powders. In general, the green density of compacts decreases with increasing milling time due to the hardening effect of mechanical milling and Fig. 4.11 reflects this at high compaction pressures where the powders milled for larger duration are found to possess lower density in comparison to those milled for relatively shorter times. However, the situation is reversed at lower pressure of compaction as evident from Fig. 4.11 where powders milled for 0 h duration show the lowest relatively density in comparison to 2, 4 and 6 h milled powders. The observed behavior can be explained on the basis of the deformation, cold

welding and fracture in conjunction with the morphology of the powders which play a vital role in packing capability of powders. One could see from Fig. 4.11 that the density of Cu4Ni-4TiC corresponding to 2 h milling duration is maximum at all the compaction pressures except at 850 MPa where the powder milled for 0 h has the largest density. It can be seen from the morphology presented in Fig. 4.6 that powders processed for 0 h have a flaky and irregular structure which influences the powder packing and the apparent density of the compact. During compaction the compressive stress is applied to the particles through the punch, the particles in touch with the punch transmit stress to the neighboring particles through the contact points between them. It has been suggested that an irregular morphology of the particles has a tendency to press forward the formation of asymmetrically opposite forces in the contact points between the particles leading to the shear distortion and consequently the cold welding of the powders. Hence, the irregular powder is harder to compact than the spherical powder as indicated by Schatt and Wieters (1997). The lower green density of the powder milled for 0 h as seen from Fig. 4.11 can be attributed to the poor packing of the dendritic and flattened powder. However, the relatively density for 0 h milled powders is the largest at the highest compaction pressure of 850 MPa used in the present study due to the enhancement in the capability of getting deformed plastically as reported by Gan et al. (2008). It appears that the applied pressures of 250, 450 and 650 MPa were sufficient enough only for inducing a little amount plastic deformation. It can be seen that at high compaction pressure i.e. 850 MPa, the green density of powders milled for 0 h, 2 h, 4 h and 6 h is 82, 79, 77 and 76%, respectively. Hence, it may be concluded that powder particles become totally deformed as well as work hardened with the increase of milling duration and possibly this can be the reason that such particles resist the compaction pressure as indicated by Gan et al.(2008). The decrease in the value of the parameter A (Table 4.3) is due to the high energy ball milling which produces work hardening effect and a change of shape of the particles from dendritic to spherical (Gan et al. 2008).

It can be observed from optical micrographs as shown in Fig. 4.13 that TiC particle are distributed in the matrix and some pores are also visible that are due to the decrease in density and agglomeration of TiC particle which tends to promote the pores formation. No cracks are observed in the micrographs. For better understanding the

microstructural features and its various aspects scanning electron micrographs and high resolution scanning electron micrographs are presented in Figs. 4.14-4.16, which show that TiC particles are distributed homogeneously in the matrix alloy. It has been reported that a uniform distribution of reinforced particles results in improvement in mechanical properties of the composites (Lee et al. 2001). The addition of relatively higher amount TiC particles results in agglomeration leading to formation of pores in the composites which could also be observed from the micrographs shown in Figs.4.14 (b) to (e) indicated by round circles. Similar, observations have earlier been reported by Rahimian et al. (2009). The agglomeration can be seen in the inset of Fig.4.14 (e). It is clear from the EDS analyses as given in Fig. 4.15 that indicate the presence of Cu, Ni, Ti, O and carbon. The small amount of oxygen in EDX spectrum may be due to the presence of an oxide layer which might have formed during sample preparation as suggested by Shorowordi et al. (2003). HR-SEM result presented in Fig. 4.16 confirms the microstructural results presented in Fig.4.13-4.15 at a high resolution. XRD pattern shown in Fig.4.17 reflects the presence of Cu-Ni and TiC, indicating the absence of any intermetallic compound formation between Cu-Ni and TiC. Similar, findings have also been reported earlier by Buytoz et al. (2014). The peaks of TiC become distinct only beyond a certain amount of its addition. The extra peaks corresponding to the presence of Ni could not be detected in the spectra as goes into making a solid solution due to complete solubility in copper (Gupta et al. 2002).

Table 4.4 and Fig. 4.18 show the effect of milling time and sintering temperature on relative density and micro-hardness behavior of Cu4Ni-4TiC. It can be observed from Table 4.4 that relative density increases as temperature increases from 800 to 850°C and then decreases as temperature increases from 850 to 900°C. In the initial stage of sintering process, when the temperature is increased from 800 to 850°C, grain growth starts and closure of the pores takes place which promotes a faster densification giving rise to a relatively dense composite. The decline in relative density beyond 850°C may be attributed to the cooling of the pellets from higher sintering temperature (900°C) which produces thermal stresses because of the disparity in the coefficient of thermal expansion (CTE) of the matrix alloy and reinforcement particles. These stresses create significant interfacial gaps and result in the decrease in relative density as indicated by Chu et al.

2010, also. At a constant sintering temperature, the density of Cu4Ni-4TiC increases till 2 h of milling beyond which it starts decreasing with increasing duration of milling as seen from Table 4.4. It may be attributed to the relatively lesser work hardening of particles due to relatively smaller milling duration of 2 h which changes the shape of particles from spherical to flattened one as discussed earlier also leading to better compaction and hence, better densification. However, when the milling duration increases the particles become totally deformed as well as work hardened resulting in a reduction in capability of getting plastically deformed which restricts the compaction and consequently results in a relatively lower densification. Similar behavior has earlier been observed by Hesabi et al. (2007).

The variation of micro-hardness with milling time for a particular temperature of sintering as given in Fig. 4.18 illustrates the similar trend of variation as shown by the relatively variation presented in Table 4.4 i.e., the hardness has been observed to be maximum for 2 h milling duration and 850°C. It may be attributed to the relatively finer size of grains in the composite milled for 2 h duration, the finer the size the better the hardness and strength. Rajkovic et al. (2014) have suggested that materials with smaller grains have more strength than materials with larger grains. Since, in the present investigation the particles milled for 2 h have smallest grains as evident from Table 4.2. Hence, it is not surprising that the composite milled for 2 h duration has shown the optimum density and hardness at 2 h milling and at a sintering temperature of 850^{o}C.

Table 4.5 and Fig. 4.19 show the effect of TiC content on relative density and micro-hardness. Both the relative density and the hardness increase with increasing TiC content up to 4 wt.%, beyond which they decrease. The increase in relative density can be attributed to the filling of pores by relatively finer TiC particles which results in an increase in relative density as reported by Khorshid et al. (2010). There are several factors which can affect the relative density of the composites. The decrease in relative density beyond a certain amount of TiC, 4 wt.% in the present study, can be attributed to the agglomeration of TiC particle as shown in Figs. 4.14 (e) and 4.16 (c) which tends to promote the pores formation and subsequent decrease in the relative density takes place (Nemati et al. 2011) resulting in a decrease in density and consequently the hardness with

increasing addition of TiC as given in Table 4.5 and Fig. 4.19. The increase in micro-hardness till 4 wt.% as shown in Fig. 4.19 may be attributed to the reinforcement of hard TiC particles. Also, since TiC particles are much harder, they resist the impressing action of the indenter better and thus provide a higher hardness. Thermal mismatch between the reinforcing TiC particles and the matrix alloy also results in internal stresses which generate the dislocations leading to an increase in the dislocation density which ultimately contributes in enhancing the micro-hardness of the composites as indicated by Tabandeh et al. (2010).

The sharp increase in the resistivity as shown in Fig. 4.20 can be attributed to non conducting nature of TiC particles which restrict the movement of electrons as they are strongly bonded to the nucleus in the carbides as suggested by Pierson, 1996. Hence, a larger amount of TiC is expected to raise the electrical resistivity which has been observed in the present study as indicated in Fig. 4.20. Other reasons for the increase in resistivity may be (i) the increase in porosity with increasing amount of non conducting phase and (ii) increase in dislocation density which intensifies the electron scattering as suggested by Buytoz et al. 2014. Since, an increase in both the porosity (due to agglomeration) and the dislocation density (due to thermal mismatch as discussed earlier) with increasing amount of TiC have been found to occur in the present study, hence, a decrease in the resistivity is not surprising. However, the dislocation density has not been quantified in the present investigation.

The effect of technological parameters on the properties of the composites presented above shows that there is an optimum milling duration, an optimum temperature and pressure of sintering to achieve the optimum density and consequently the hardness in the P/M processed composites. The study also reveals that it is the uniform distribution of second phase rather than its amount which plays a vital role in attaining the desired properties in such composites. This has been confirmed by the higher density and hardness shown by the composite containing 4 wt. % of TiC rather than those containing 6 and wt.% TiC, respectively, because of the agglomeration of particles in these composites.